SPATIAL REDISTRIBUTION OF PERFUSION AND GAS EXCHANGE IN PATIENT-SPECIFIC MODELS OF PULMONARY EMBOLISM

MH Tawhai[1], AR Clark[1], ML Wilsher[3], DG Milne[2], K Subramaniam[1], KS Burrowes[4]

[1]Auckland Bioengineering Institute, and [2]Anatomy with Radiology, University of Auckland, Private Bag 92019, Auckland 1142, New Zealand.
[3]Respiratory Services, Auckland District Health Board, Private Bag, 92024, Auckland, New Zealand.
[4]Department of Computer Science, University of Oxford, Wolfson Building, Parks Road, Oxford, UK.

ABSTRACT

The most common cause of acute pulmonary hypertension is pulmonary embolism (PE). Classification of PE severity can be based on obstruction indices that are estimated from clinical imaging, however, as patients with apparently similar levels of obstruction can have quite different clinical outcomes, obstruction indices currently have limited use clinically. Embolus size and location affects patient response, as well as the existance of prior pulmonary disease, but neither of these factors is accounted for in current obstruction indices. To fully assess the importance of embolus size and location, patient-specific models of the functional response to PE must be matched to individual clinical outcomes. Here we describe the use of patient-specific imaging-based models of PE to provide insight into the mechanisms that are important in determining PE severity, and to correlate pathology with (dys)function.

Index Terms— Biological system modeling, Biomedical image processing, Medical diagnosis

1. INTRODUCTION

Acute thromboembolic pulmonary embolism (PE) can elevate pulmonary vascular resistance (PVR) and hence over load the right ventricle (RV), leading to cardiac failure and/or chronic pulmonary hypertension (PH) via remodeling of the RV and pulmonary vasculature. The degree of arterial occlusion can be quantified using 'obstruction indices' (OIs) which take into account the anatomical location of the emboli and their size. However these indices have not been adopted in routine clinical practice because they do not correlate with clinical outcome. Current methods for estimating OIs neglect the spatial distribution of the emboli, which could be important in determining the integrated response of the perfusion and gas exchange systems.

PH is defined as elevation of pulmonary artery pressure (PAP) to greater than 25 mmHg at rest [1]. While vasoconstriction has been suggested as an important mechanism in elevating PVR in animal studies - presumably due to release of mediators from the thrombus [2] - this operates in a system where very large portions of the capillary bed are unperfused. How the degree of obstruction and its distribution impacts on PH is not known, however we have previously shown that occlusion of the vasculature by multiple emboli is generally insufficient to elevate the PAP to PH levels when the subject is at rest, due to the ability of the lung to redistribute flow and distend or recruit non-occluded capillaries [3]. As the pulmonary circulation remains relatively inaccessible to measurement, we have developed a multi-scale model that simulates the distribution of blood in the lung and regional gas exchange under baseline conditions and following placement of emboli. The model is customised to individual patient imaging and pulmonary function data. Here we present a methodology to map clinical CTPA imaging to a computational model of PE, and correlate patient outcomes with embolus distribution.

2. METHODS

We present a method for relating computed tomography pulmonary angiograms (CTPAs) to patient-specific function in acute PE based on clinical data.

2.1. Patient Data

Volumetric CTPAs were obtained from 9 adult subjects presenting with clinically suspected acute PE at Auckland City Hospital. The Northern X Regional Ethics Committee and the Auckland District Health Board Research Review Committee approved use of the clinical data. Patients underwent pulmonary function testing following recruitment into the study, to confirm that their lung function was otherwise normal hence avoiding the complication of prior pulmonary disease worsening patient outcomes.

2.2. Geometric Models

For each patient the lungs, lobes, central airways and large intra-pulmonary blood vessels were segmented automatically from CTPAs using custom built software

(PASS, Pulmonary Analysis Software Suite, University of Iowa [4, 5]). The arterial trunk (the blood vessels that lie between the two lungs) cannot be automatically segmented using PASS. These vessels were manually segmented from the CTPAs within the framework of this software.

2.2.1. Blood vessel and airway geometries

A one-dimensional finite element tree was constructed to represent each of the arterial, venous and airway trees [6-8]. Airways, arteries and veins were identified from segmented imaging data to the level of the first sub-segmental branches. A geometry representing the centerlines of each of these vessels was then constructed using the CMGUI software (www.cmgui.org). Beyond this level the airway and vascular segmentation have reduced reliability and segmentation software may not capture each bifurcation. Therefore, vessels distal to the first sub-segmental branches were generated using a volume filling branching algorithm [8] that aims to create a tree structure which fills a prescribed volume and matches as closely as possible the properties of measured pulmonary trees. The volume into which the airways and vessels were grown was that of the patient's lobes, as obtained from the PASS segmentation of their CTPAs. Figure 1 illustrates how the blood vessel geometry constructed for an individual corresponds to their CTPA. The trachea and main pulmonary venous diameters were measured from the CTPA to include as much patient specificity as possible. Main pulmonary artery diameters in PE are larger than one would expect due to higher than normal blood pressures, so baseline (unstrained) diameters were scaled from normal data [9] based on the patient's venous diameter. Diameter ratios were used to define intermediate vessel and airway diameters such that order 1 vessels were of a size measured in normal subjects [9, 10].

2.2.2. Embolus Identification.

Emboli were identified in each patient by a radiologist (DGM) (Figure 2a). Then a semi-automated procedure was implemented to identify the three dimensional distribution

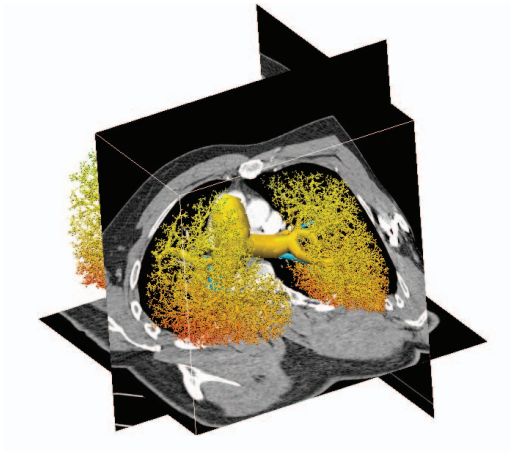
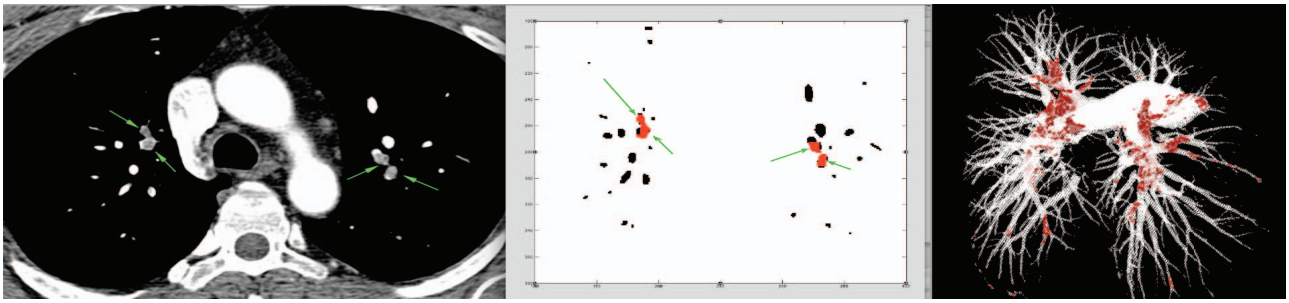


Figure 1: A geometric model of the pulmonary vasculature obtained from CTPA data in one patient.

of emboli (Figure 2c) and allow mapping of each embolus to the blood vessel in which it resides. As CTPAs are contrast enhanced the pulmonary blood vessels can be identified via their high pixel values. Figure 2a shows a CTPA slice with radiologist-identified emboli indicated by arrows. Emboli are associated with a lower pixel value than their surrounding blood vessels and therefore can be extracted from imaging data. However, false positives can occur in automatic detection of emboli as vessel walls, bifurcations and some pulmonary veins can present with similar pixel values to emboli [11].

The algorithm used to detect pulmonary emboli used here was implemented in MATLAB® (Version 2011a, The Mathworks Inc.). The CTPA images, lung masks and central artery masks created using PASS were imported into MATLAB. The region of the images external to the lung and arterial mask was subtracted from the images and discarded from analysis. An erosion filter was used to remove noise from the edges of the lung mask. As the automated vessel segmentation acquired from PASS



(a) **(b)** **(c)**

Figure 2: Results of the algorithm designed to extract emboli from CTPA. The image shows (a) radiologist identified emboli (green arrows) in a CTPA slice, (b) the output of the semi-automated identification of emboli (red arrows) in the same slice, and (c) a 3D map of blood vessels (white) and emboli (red).

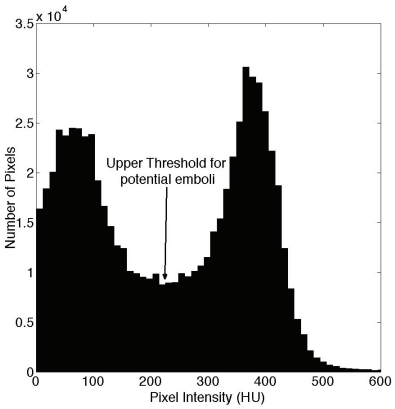


Figure 3: A pixel intensity histogram which shows two distinct peaks. The first peak (lower intensities) comprises emboli, vessel walls, bifurcations and some veins. The second (higher intensities) comprises contrast-enhanced blood.

contained 'holes' in place of emboli, potential emboli were identified as pixels within the lung boundary with a Hounsfield unit (HU) value greater than zero. A histogram analysis of each image set shows a bimodal distribution of pixel intensities greater than 0HU (Figure 3). The first peak corresponds to potential emboli and the second to (contrast-enhanced) unoccluded blood vessels. The location of the trough for each patient's histogram was used as an upper intensity limit for potential emboli. These potential emboli include vessel walls, veins and small regions of parenchymal tissue so a smoothing and thresholding step was applied to reduce the number of false positives.

All pixel values that were not identified as potential emboli were set to zero value, and the lung was split into 4x4x4 mm rectangular voxels. The mean pixel value in each voxel was calculated and compared to the mean pixel value of all potential emboli. When a voxel intensity value was less than 50% of the overall mean value the pixels that represent potential emboli within that voxel were neglected. This removes small clusters of potential emboli which reduces the number of vessel wall regions and bifurcations that are falsely identified by the algorithm. Very small emboli are also removed in this smoothing, but the voxel size was set at a small enough resolution that all radiologist-identified emboli were captured in each subject. Figure 3 shows the results of the algorithm compared with radiologist-identified emboli and a 3D map of potential emboli.

Emboli were mapped to arterial vessels, constructed as described in Section 2.2.1, using CMGUI. In this step, false positives due to pulmonary veins neglected. Then, the effective volume of vessel lumen and embolus (number of pixels x pixel spacing x slice separation) associated with each artery was calculated. From these calculations an effective embolus radius was calculated, assuming that the embolus spans the length of the vessel that it occludes.

2.3. Functional Models

Perfusion, ventilation and gas transfer were simulated in each patient using previously described methods [3, 12, 13]. Cardiac output and tidal volumes were specified based on height, age and weight. The metabolic rate at rest, and undergoing fidgeting or walking was calculated from the formulae of Levine et al [14], and translated to an oxygen consumption rate and ventilation rate [15]. Finally, cardiac output was calculated using the results of Stringer et al [16].

Perfusion was simulated using a steady-state model of blood flow [12]. This model assumes Poiseulle flow in elastic extra-capillary blood vessels and a symmetric intra-acinar structure with capillary sheets connecting each generation of blood vessels. Parenchymal tissue deformation is accounted for by assuming a linear gradient of pleural pressure in the direction of gravity.

Ventilation was simulated using the quasi-static model of Swan et al [13]. This model assumes Poiseuille flow in extra-acinar airways coupled to a lumped parameter description of the acinus. Flow is driven by a change in pleural pressure acting externally to the lung, which varies linearly with vertical height.

Oxygen transfer from air to blood was simulated as in Burrowes et al. [3]. The model assumes equilibration of oxygen in the air and blood, which is valid unless blood flow transit through the capillary bed takes less than 0.25s.

2.3.4. Embolus Occlusion

Emboli were assumed to be solid occlusions with radii as estimated in Section 2.2.2. The effective radius of a vessel was then the perfused radius of the elastic vessel minus the radius of the embolus. This acts to decrease the effective radius of an occluded vessel, resulting in an increased blood pressure and potential expansion of the vessel around the embolus. If a measured embolus radius was equal to that of its enclosing vessel, blood flow was assumed negligible through that vessel. Systemic oxygen requirements were assumed to remain the same pre- and post-embolization and venous oxygen content was recalculated post-embolization to satisfy this requirement.

3. RESULTS AND CONCLUSIONS

Baseline simulations in the upright posture (at rest) predicted a mean PAP (mPAP) across subjects of 14.8±0.9 mmHg and a PVR of 1.0±0.2 Wood units. Mean arterial oxygen (PaO_2) was predicted to be 96.0±1.8 mmHg. Post-embolus occlusion mPAP was predicted to increase to 19.1±2.8 mmHg (PVR=2.0±0.6 Wood units) and PaO_2

reduced to 69.3±18.6 mmHg. No simulations predicted hypertensive levels; however, 5 of the 9 subjects had a predicted PaO_2<80 mmHg. These results confirm previous findings [3] that occlusion alone is insufficient to elevate mPAP to hypertensive levels.

Previously [3] we have proposed that hypoxic pulmonary vasoconstriction (HPV) may be a significant contributor to increases in PVR in PE. RV dysfunction was reported in all patients with predicted post-embolus PaO_2<80 mmHg, and none of the patients with PaO_2>80 mmHg. All patients with RV dysfunction had a significant proportion of alveoli with P_AO_2<80 mmHg. As HPV acts predominantly on small pulmonary arteries this supports the previous findings that HPV may play a significant role in response to PE.

An advantage of the subject-specific boundary conditions used here is that the response to elevated cardiac output in PE can be assessed quantitatively. Three of the subjects presented with tachycardia (heart rate > 100 bpm). Whether this increased heartrate is a response to reduced PaO_2 (each subject with tachycardia had a predicted PaO_2<80 mmHg) or stress-related is unknown. Figure 4 shows pre- and post-occlusion curves relating pulmonary artery pressure to cardiac output for one of these subjects. This subject meets the definition of PH at rest for a cardiac output of 8.6 l/min. According to the data of Levine et al [14], one would expect the cardiac output of this subject to reach 8.56 l/min when fidgeting upright. Therefore it is feasible that stress may elevate PAP to PH levels in some subjects even in the absence of HPV.

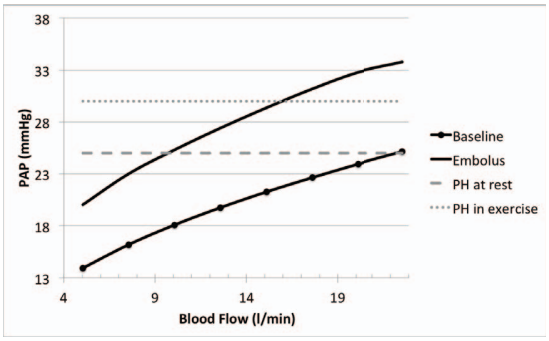


Figure 4: Predicted PAP versus flow curves pre- and post embolus occlusion for a single patient considered in this study.

4. REFERENCES

[1] Galie, N., et al., "Guidelines on diagnosis and treatment of pulmonary arterial hypertension. The Task Force on Diagnosis and Treatment of Pulmonary Arterial Hypertension of the European Society of Cardiology.". *Eur Heart J*. 25: pp. 2243-2278, 2004.

[2] Smulders, Y.M., "Pathophysiology and treatment of haemodynamic instability in acute pulmonary embolism: the pivotal role of pulmonary vasoconstriction". *Cardiovasc Res*. 48: pp. 23-33, 2000.

[3] Burrowes, K.S., A.R. Clark, and M.H. Tawhai, "Blood flow redistribution and ventilation-perfusion mismatch during embolic pulmonary occlusion". *Pulm Circ*. 1(3): pp. 365-376, 2011.

[4] Hoffman, E.A., et al., "The comprehensive imaging-based analysis of the lung: a forum for team science (1)". *Acad Radiol*. 11(12): pp. 1370-1380, 2004.

[5] Hu, S., E.A. Hoffman, and J.M. Reinhardt, "Automatic lung segmentation for accurate quantitation of volumetric X-ray CT images". *IEEE Trans Med Imag*. 20(6): pp. 490-8, 2001.

[6] Burrowes, K.S., P.J. Hunter, and M.H. Tawhai, "Anatomically-based finite element models of the human pulmonary arterial and venous trees including supernumerary vessels". *J Appl Physiol*. 99: pp. 731-738, 2005.

[7] Tawhai, M.H., et al., "CT-based geometry analysis and finite element models of the human and ovine bronchial tree". *J Appl Physiol*. 97(6): pp. 2310-2321, 2004.

[8] Tawhai, M.H., A.J. Pullan, and P.J. Hunter, "Generation of an anatomically based three-dimensional model of the conducting airways". *Ann. Biomed. Eng.* 28(7): pp. 793-802, 2000.

[9] Huang, W., et al., "Morphometry of the human pulmonary vasculature". *J Appl Physiol*. 81(5): pp. 2123-2133, 1996.

[10] Horsfield, K. and G. Cumming, "Morphology of the bronchial tree in man". *J Appl Physiol*. 24: pp. 373-383, 1968.

[11] Masutani, Y., H. MacMahon, and K. Doi, "Computerized detection of pulmonary embolism in spiral CT angiograpghy based on volumetric image analysis". *IEEE Trans Med Imag*. 21(12): pp. 1517-1523, 2002.

[12] Clark, A.R., M.H. Tawhai, and K.S. Burrowes, "The interdependent contributions of gravitational and structural features of the lung to the distribution of pulmonary perfusion in a multi-scale model of the pulmonary circulation". *J Appl Physiol*. 110: pp. 943-945, 2011.

[13] Swan, A.J., A.R. Clark, and M.H. Tawhai, "A computational model of the topographic distribution of ventilation in healthy human lungs". *J Theoret Biol*. In Press, 2011.

[14] Levine, J.A., S.J. Schleusner, and M.D. Jensen, "Energy expenditure of nonexercise activity". *Am J Clin Nutrit*. 72: pp. 1451-1454, 2000.

[15] Weir, J.B.d.V., "New methods for calculating metabolic rate with special reference to protein metabolism". *J Physiol*. 109: pp. 1-9, 1949.

[16] Stringer, W.W., J.E. Hansen, and K. Wasserman, "Cardiac output estimated noninvasively from oxygen uptake during exercise". *J Appl Physiol*. 82: pp. 908-912, 1996.